

Article

Susceptibility Mapping of Typical Geological Hazards in Helong City Affected by Volcanic Activity of Changbai Mountain, Northeastern China

Xiaohui Sun ^{1,†}, Chenglong Yu ^{2,3,4,†}, Yanrong Li ^{1,*} and Ngambua N. Rene ¹

¹ Department of Earth Sciences and Engineering, Taiyuan University of Technology, Taiyuan 030024, China; sunxh17@mails.jlu.edu.cn (X.S.); lenei0069@link.tyut.edu.cn (N.N.R.)

² Changchun Institute of Technology, College of Jilin Emergency Management, Changchun 130012, China; yucl16@mails.jlu.edu.cn

³ Jilin Team of Geological Survey Center of China Building Materials Industrial, Changchun 130026, China

⁴ College of Construction Engineering, Jilin University, Changchun 130026, China

* Correspondence: li.dennis@hotmail.com; Tel.: +86-18204318089

† These authors contributed equally to this work.

Abstract: The purpose of this paper was to produce the geological hazard-susceptibility map for the Changbai Mountain area affected by volcanic activity. First, 159 landslides and 72 debris flows were mapped in the Helong city area based on the geological disaster investigation and regionalization (1:50,000) project of Helong City. Then, twelve landslide conditioning factors and eleven debris flow conditioning factors were selected as the modeling variables. Among them, the transcendental probability of Changbai Mountain volcanic earthquake greater than VI degrees was used to indicate the relationship between the geological hazard-susceptibility and Changbai Mountain volcanic earthquake occurrence. Furthermore, two machine learning models (SVM and ANN) were introduced to geological hazard-susceptibility modeling. Receiver operating characteristic curve, statistical analysis method, and five-fold cross-validation were used to compare the two models. Based on the modeling results, the SVM model is the better model for both the landslide and debris flow susceptibility mapping. The results show that the areas with low, moderate, high, and very high landslide susceptibility are 31.58%, 33.15%, 17.07%, and 18.19%, respectively; and the areas with low, moderate, high, and very high debris flow susceptibility are 25.63%, 38.19%, 23.47%, and 12.71%, respectively. The high and very high landslide and debris flow susceptibility classes make up 85.54% and 80.55% of the known landslides and debris flow, respectively. Moreover, the very high and high landslide and debris flow susceptibility are mainly distributed in the lower elevation area, and mainly distributed around the cities and towns in Helong City. Consequently, this paper will be a useful guide for the deployment of disaster prevention and mitigation in Helong city, and can also provide some reference for evaluation of landslide susceptibility in other volcanically active areas.

Keywords: geological hazard-susceptibility mapping; Changbai Mountain; volcanic earthquake; transcendental probability



Citation: Sun, X.; Yu, C.; Li, Y.; Rene, N.N. Susceptibility Mapping of Typical Geological Hazards in Helong City Affected by Volcanic Activity of Changbai Mountain, Northeastern China. *ISPRS Int. J. Geo-Inf.* **2022**, *11*, 344. <https://doi.org/10.3390/ijgi11060344>

Academic Editors: Wolfgang Kainz and Godwin Yeboah

Received: 25 April 2022

Accepted: 8 June 2022

Published: 10 June 2022

Publisher's Note: MDPI stays neutral with regard to jurisdictional claims in published maps and institutional affiliations.



Copyright: © 2022 by the authors. Licensee MDPI, Basel, Switzerland. This article is an open access article distributed under the terms and conditions of the Creative Commons Attribution (CC BY) license (<https://creativecommons.org/licenses/by/4.0/>).

1. Introduction

Changbai Mountain, located in the southeast of Jilin Province, is an important tourist attraction in northeast China. Once the Tianchi Volcano of Changbai Mountain becomes active again and erupts, the seismic force caused by the associated earthquake will lead to geological disasters in the Changbai Mountain area, resulting in the loss of life and property and affecting the development of the region [1]. According to the monitoring results of Tianchi Volcano in Changbai Mountain, from 2002 to 2005, the magnitude of earthquakes associated with Tianchi Volcano, topographic changes, earthquake frequency, and greenhouse gas emissions showed a clear increasing trend, and the frequency of

earthquakes even reached a peak of more than 1200 times in the year 2003. In addition, in May 2010, the height change of the northern slope of the Tianchi volcano cone reversed, with a sudden drop of 12.72 mm, breaking the rule of an annual increase of 4 mm [2]. The above monitoring results indicate that Tianchi volcano is likely to enter an active period. Therefore, it is necessary to carry out susceptibility mapping of geological hazards caused by Tianchi volcanic activity.

Susceptibility to geological disasters refers to the spatial probability and intensity of geological disasters occurring in a specific area within a certain period [3–5]. It is a reflection of the natural attributes of geological disasters under the action of internal and external factors and can be described by the susceptibility index (0–1) [6]. This index is used to evaluate the problem of “where and what combination of geological environment conditions are most prone to geological disasters” [7–9]. It mainly focuses on the basic geological conditions of existing or potential geological disasters, such as landform, rock and soil type, meteorology and hydrology, human activities, etc., and predicts the probability of geological disasters, that is, the tendency for the occurrence of geological disasters. From a review of the relevant literature, the susceptibility mapping process of geological disaster can be roughly divided into the following four parts: [10–12]: (a) Acquisition of geological disaster inventory data: This is the basis of geological disaster-susceptibility mapping [13–15]. Nowadays, the method of geological disaster interpretation with the integration of “space–sky–ground” has become an important part of geological disaster inventory data acquisition [16–20]. (b) Mapping unit selection: The mapping unit is the (minimum indivisible) basic unit of geological disaster-susceptibility mapping, and has the characteristics of homogeneity within units and heterogeneity between units [8,21]. Nowadays, grid units, slope units, watershed units, and so on, have become the commonly used mapping units. (c) Establishment of evaluation index system: The evaluation index system is another key issue for geological disaster-susceptibility mapping. At present, most studies are based on expert experience, cause analysis and detailed field survey, and the indexes with high correlation with the geological disaster occurrence are selected as the evaluation index [22]. (d) Selection of susceptibility model: With the development of computer technology and mathematical models, the number of models applied to geological disaster risk regionalization is gradually increasing. These models can be roughly divided into two types, those using a qualitative evaluation method and those using a quantitative evaluation method through classification and summary [23]. The qualitative evaluation method uses the expert experience of geologists to realize the geological hazard-susceptibility mapping by assigning weights and scoring [24–26], such as the analytic hierarchy process [27]. Nowadays, there are more and more applications of quantitative analysis, such as the most common binary statistics method [28–34], the evidence-weight method and so on [35,36]. Machine learning algorithms and data mining algorithms are also increasingly introduced into geological hazard-susceptibility mapping [37], such as support vector machine models [38].

In this study, geological hazard-susceptibility mapping, including landslide and debris flow, was carried out in Helong city, which is located northeast of the Changbai Volcano. First, the geological hazards were mapped in the Helong city. Then, the slope unit and watershed unit were selected as the mapping unit. The transcendental probability of Changbai Mountain volcanic earthquake greater than VI degrees was used to indicate the relationship between the geological hazard-susceptibility and Changbai Mountain volcanic earthquake. Eleven other landslide conditioning factors and ten other debris flow conditioning factors were also selected as the evaluation factors. Two models, an SVM model and an ANN model, were then compared and evaluated by using the receiver operating characteristic curve, statistical analysis method, and five-fold cross-validation.

2. Study Area

Helong city is a county-level city under the jurisdiction of Yanbian State, located in the southwest of Yanbian State and the north bank of the upper reaches of Tumen River

at the eastern foot of Changbai Mountain (Figure 1a,b). The city ranges from $128^{\circ}22'42''$ to $129^{\circ}24'17''$ E longitude and $41^{\circ}59'44''$ to $42^{\circ}57'15''$ N latitude. It is about 100 km long from north to south and 70 km wide from east to west, with a total area of 5068.62 km². Helong city is located in the northeast of the Changbai Mountains, and its ground gradually decreases from southwest to northeast. The southwest is high and steep, the middle is hilly, and the northeast is relatively flat. The climate type of Helong city is the middle temperate monsoon sub-humid climate zone. It is characterized by four distinct seasons, with fickle cold and warm springs, short and not very hot summers, mild and cool autumns with many sunny days, and long cold winters. Based on the geological map, with a scale of 1:250,000, there are six strata exposed in Helong city, namely Quaternary (Q), Neogene (N), Cretaceous (K), Jurassic (J), Mesoproterozoic (Pt), and Archaean (Ar) (Figure 1c).

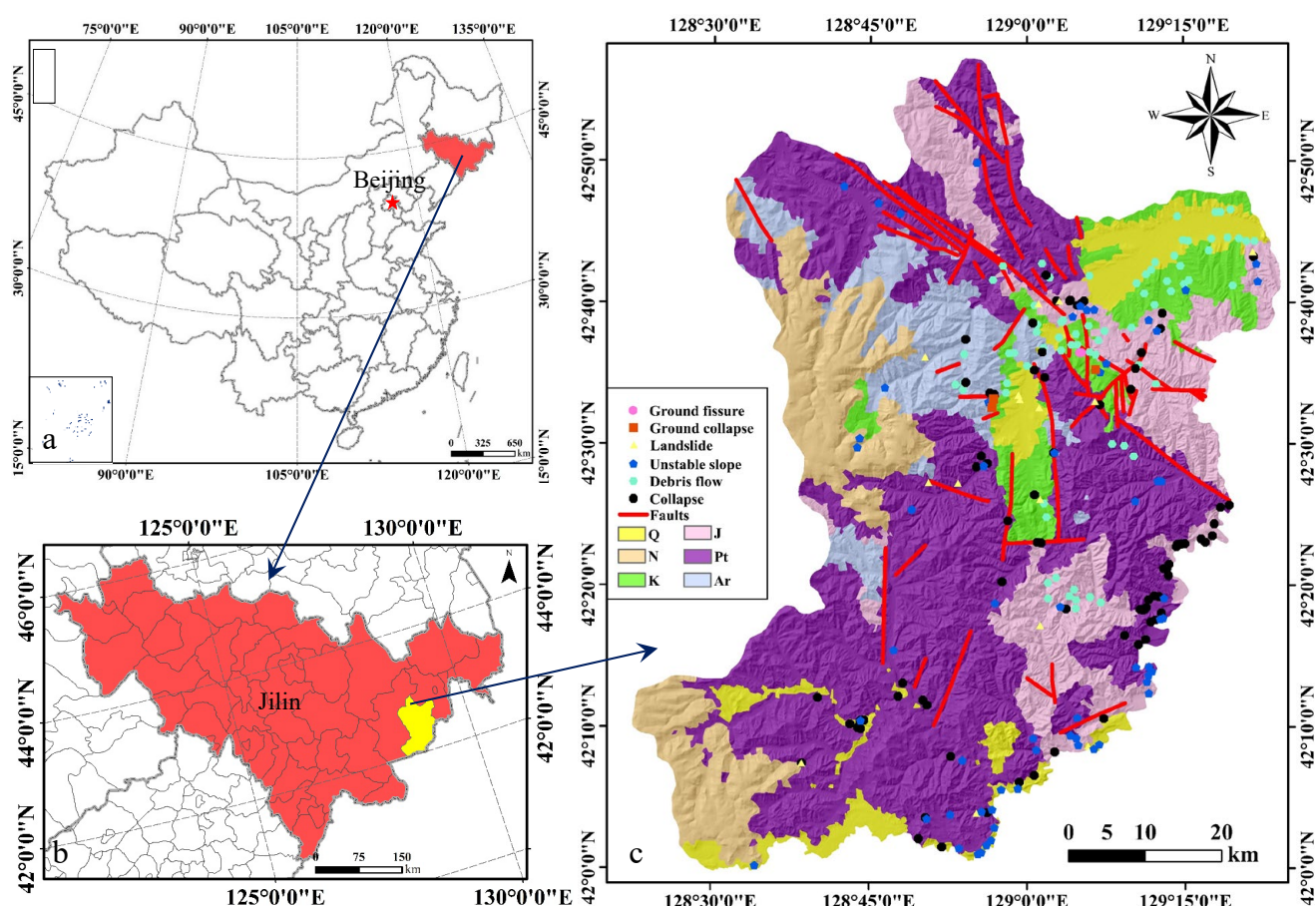


Figure 1. Location of the study area (a,b) and geological hazard inventory map and geological map (c).

According to the volcano monitoring of Changbai Mountain (Tianchi Volcano monitoring station of Changbai Mountain), since 2002, the seismic activity associated with volcanic activity of Changbai Mountain began to rise significantly reaching a peak in 2003, and the number of earthquakes caused by volcanic activity of Changbai Mountain might have been as high as 1293 [1]. Moreover, from 2002 to 2005, the elevation of the Cone of Tianchi volcano acquired an additional 86.13 mm, more than 3 times the previous increase, and returned to normal after 2005. Since 2010, the vertical elevation of the volcanic cone on the northern slope of Tianchi Mountain has been abnormal again, with a sudden drop of 12.72 mm [2]. Although the above events do not indicate that the volcanic activity of Changbai Mountain has entered an active period, the frequent volcanic activity will certainly affect the stability of the surrounding slope and geological body.

3. Methods and Data

3.1. Geological Hazard Inventory Data

First, the detailed geological hazard inventory data should be obtained. The accuracy of mapping results is greatly affected by the degree of detail in the geological hazard inventory data. [8]. The geological disaster inventory data in this paper are from the geological disaster investigation and regionalization (1:50,000) project of Helong City, Jilin Province implemented by the Jilin Branch of China Building Materials Industrial Geological Exploration Center. Using remote sensing interpretation, ground survey, geophysical exploration, drilling, and other means, the project identified 236 geological disaster points in Helong City, including debris flow, landslide, collapse, unstable slope, ground fissures, and ground collapse. The number and proportion of various geological disasters are enumerated in Table 1, and the distribution characteristics of various geological disasters are shown in Figure 1c. Table 1 shows that the ground fissures and ground collapse only account for 2.12% of the total geological disasters in Helong city, and these two kinds of geological disasters are caused by mining activities. Thus, the typical geological disasters in Helong city are landslide (6.78%), collapse (33.90%), unstable slope (26.69%), and debris flow (30.51%). According to the similarity principle of genetic mechanism and mapping unit suitability, collapse, landslide, and unstable slope are collectively referred to as landslide geological hazards in this study. Due to the difference in the influencing factors, this paper will study the susceptibility mapping of landslide (including collapse, landslide, and unstable slope) and debris flow, respectively.

Table 1. List of geological hazards in the study area.

Type	Collapse	Debris Flow	Unstable Slope	Landslide	Ground Collapse	Ground Fissures	Total
Number	80	72	63	16	3	2	236
Ratio (%)	33.90	30.51	26.69	6.78	1.27	0.85	100

3.2. Mapping Unit

Appropriate selection of mapping units is the key factor for reasonable mapping results. Nowadays, there are five commonly used mapping units [8,9], namely: (a) Grid units, for which the data structure is very simple and the calculation is fast, but it lacks the connection with the basic terrain features. (b) Watershed unit, classification by regional watershed line being suitable for susceptibility mapping of debris flow, which itself is greatly affected by flow threshold. (c) Slope unit, or classification by watershed line and catchment line, which is a further subdivision of watershed unit, and is suitable for landslide susceptibility mapping. (d) Regional units, or classification by administrative boundaries, which are suitable for disaster prevention and mitigation based on administrative divisions. (e) Uniform conditional unit, which is classification by specific layer, is layer independent, and is easy to calculate. The typical geological disasters in Helong city are debris flow, landslide, collapse, and unstable slope. Considering the applicability of different mapping units, the susceptibility of debris flow and landslide (including landslide, collapse, and unstable slope) is mapped by selecting watershed units and slope units respectively. The classification of watershed units is based on the realization of the hydrological analysis function of GIS software. By setting different flow thresholds, the optimal classification results are optimized. Because the curvature watershed method is more concentrated in the area of slope units and has better uniformity within the units, this paper selects this method for the classification of slope units. The optimization of slope unit results is realized by setting different DEM (Digital Elevation Model) resolutions. The division process of the mapping unit is shown in Figure 2.

In this paper, a DEM with a resolution of 8.30 m, downloaded from 91 *Weitu* software (Version number: V18.8.8, Creator: Beijing Qianfan Shijing Technology Co., LTD, Location: Beijing, China), is used to classify the mapping units. In order to obtain reasonable mapping unit division results, the resolution of DEM is converted to 30 m, 50 m, 70 m, 100 m, 130 m,

150 m, 180 m, 200 m, 230 m, 250 m, respectively, for slope unit division; and the flow threshold is set to 3000, 5000, 8000, 10,000, 12,000 and 15,000 for watershed unit division, respectively. By comparing the above mapping unit division results with Google image, it is found that the mapping unit division results are most reasonable when the DEM resolution is 200 m and the flow threshold is 10,000. A total of 9574 slope units were classified, with the largest and smallest units covering 3.15 km² and 0.11 km², respectively. As for the watershed unit, a total of 2133 units were classified, and the largest watershed unit is 17.78 km², and the smallest is 0.21 km². The mapping unit classification results are shown in Figure 3.

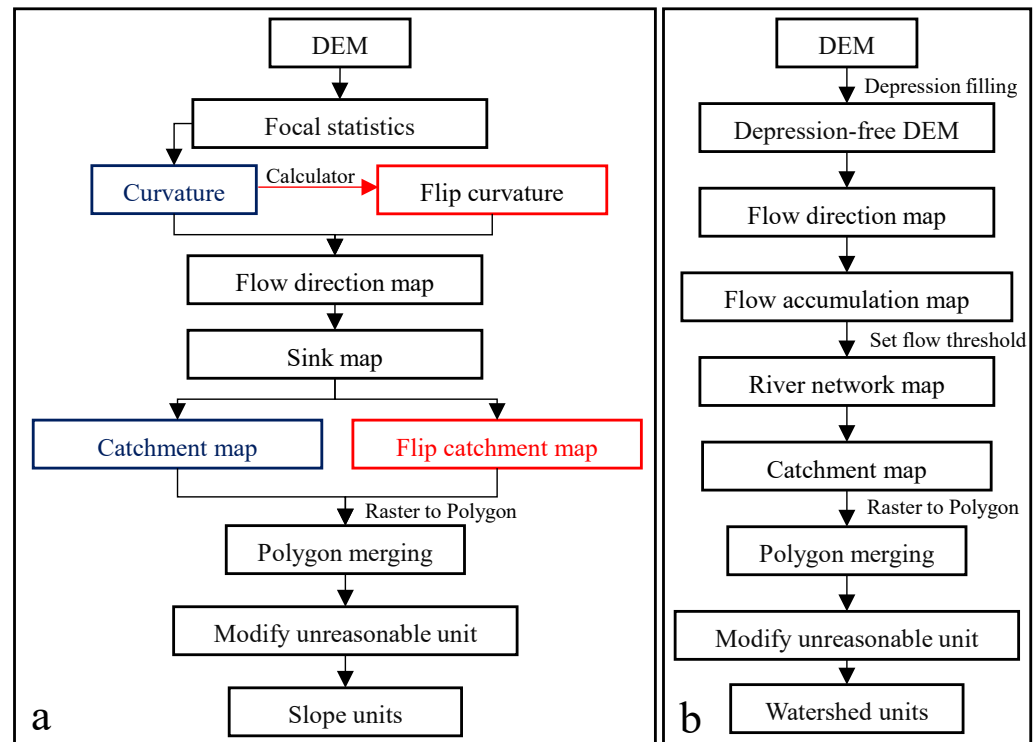


Figure 2. Division process of the mapping unit: (a) slope unit; and (b) watershed unit.

3.3. Conditioning Factors

3.3.1. Establishment of the Conditioning Factors System

The selection of evaluation indexes is one of the key issues in the study of geological hazard-susceptibility mapping. At present, the selection of conditioning factors mostly relies on the field investigation, formation mechanism analysis, expert experience, and related research on geological disasters; and the factors with the highest correlation with the occurrence of geological disasters are selected [22]. In 2017, Pourghasemi and Rossi [22] carried out statistical analysis on the application times of conditioning factors selected from 220 related pieces of research in the literature published from 2005 to 2012. According to the statistical results, the factors that were most frequently used were slope angle, lithology, slope aspect, land use, distance from the river, elevation, distance from the faults, plan curvature, profile curvature, and distance from road (top ten). Moreover, the special geological environment in the study area, notably volcanic earthquakes, should also be taken into special consideration. Thus, twelve conditioning factors (Figure 4) are selected for the landslide susceptibility mapping, namely geology (L_1), slope angle (L_2), slope aspect (L_3), topographic relief (L_4), curvature (L_5), distance to fault (L_6), land use (L_7), average annual rainfall (L_8), distance to the river (L_9), distance to the road (L_{10}), basic earthquake intensity (L_{11}), and volcanic earthquake (L_{12}).

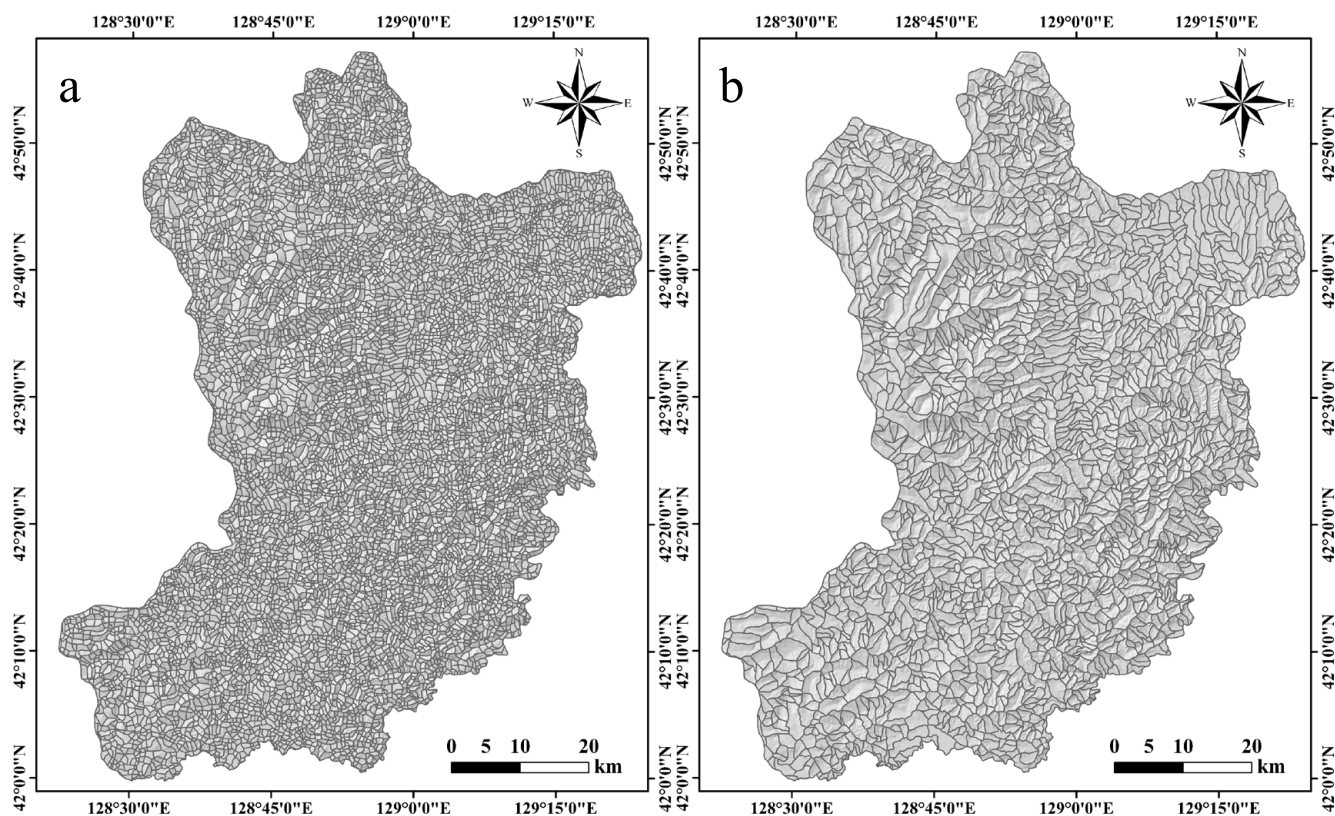


Figure 3. The mapping unit classification results: (a) slope unit, and (b) watershed unit.

The occurrence of debris flow is a complex process, and the factors affecting its occurrence are different in different regions. Based on the statistics by Niu et al. [39] of the application frequency of conditioning factors for susceptibility mapping of debris flow, the slope angle, area, slope aspect, lithology, land use, rainfall, and elevation difference are the most frequently used factors. Taking the geological environment characteristics of the study area into consideration, eleven conditioning factors are selected for debris flow susceptibility mapping (Figure 5), namely: geology (DB_1), slope angle (DB_2), slope aspect (DB_3), area (DB_4), basin elevation difference (DB_5), roundness (DB_6), distance to fault (DB_7), land use (DB_8), average annual rainfall (DB_9), geomorphic information entropy (DB_{10}), and volcanic earthquake (DB_{11}).

The data sources and the mutator methods of each conditioning factor to the mapping unit are shown in Table 2. This paper only introduces the extraction of volcanic seismic factors in detail.

The magma chamber of Changbai Mountain is less than 10 km deep, and the volcanic earthquakes caused by the volcanic activities of Changbai Mountain are usually shallow earthquakes, which have a great influence on the stability of the slope. According to the current monitoring data of Changbai Mountain, since 2003, the frequency and magnitude of volcanic earthquakes have been increasing, and the temperature of spring water in Tianchi lake has also increased significantly. Expertgeologists believe that the Changbai mountain volcano sthe potential for an eruption. The study area is only 70 km away from Changbai Mountain. The active and frequent seismic activities may affect the stability of geological disasters. Liu (2016) [1] used the transcendental probability of volcanic earthquake intensity greater than VI degrees to represent the influence of Changbai Mountain volcanic earthquake on regional rock and soil stability. This study also extracted volcanic earthquake factors according to the calculation principle of Liu (2016) [1]. The transcendental probability of Changbai Mountain volcanic earthquake intensity greater than VI degree is calculated as follows:

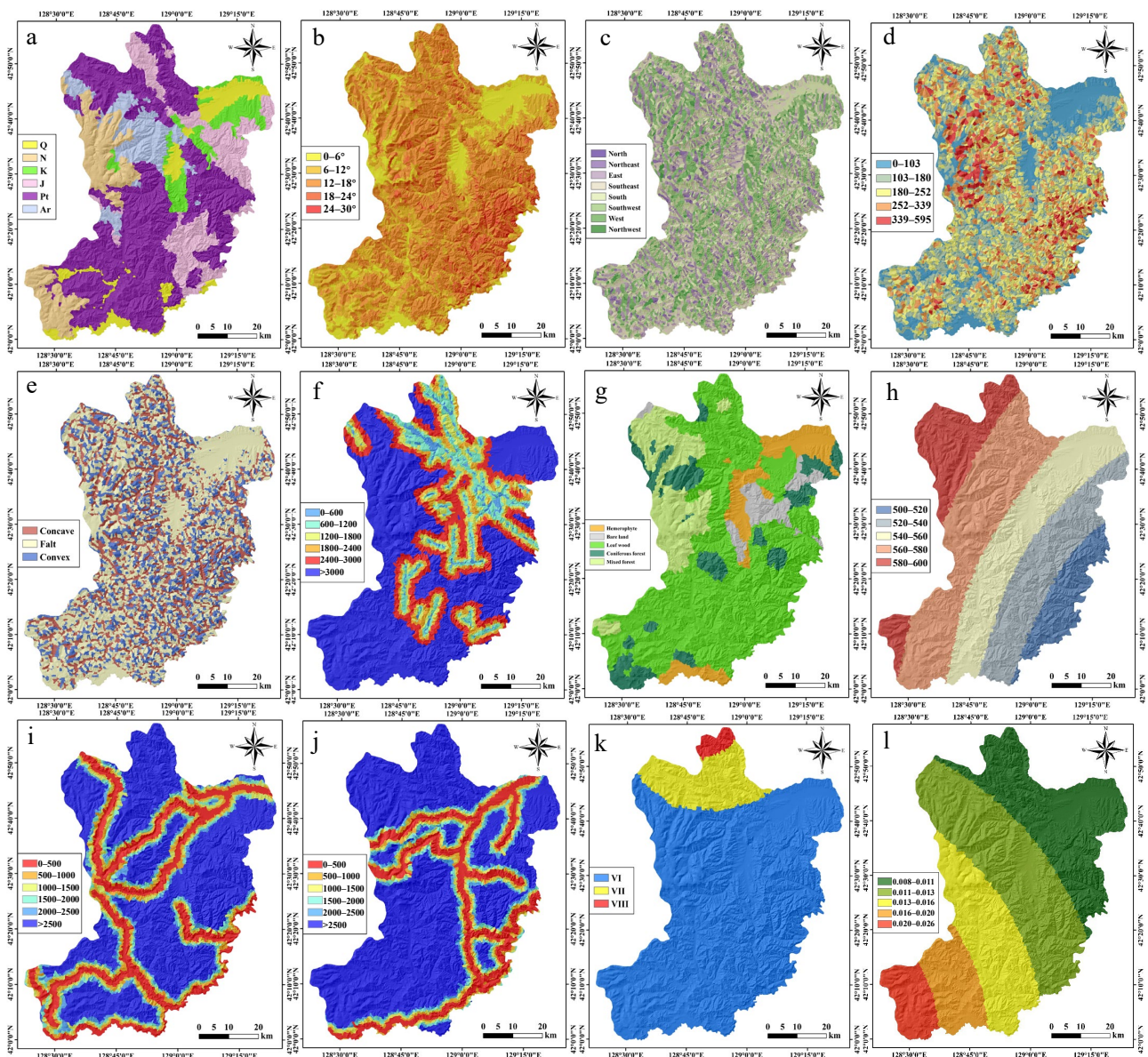


Figure 4. The conditioning factors for landslide susceptibility mapping: (a) geology, (b) slope angle, (c) slope aspect, (d) topographic relief, (e) curvature, (f) distance to fault, (g) land use, (h) average annual rainfall, (i) distance to river, (j) distance to road, (k) basic earthquake intensity, and (l) volcanic earthquake.

(1) Estimation of the magnitude of earthquakes associated with volcanic activity in Changbai Mountain. The Gutenberg-Richter theory is widely used in seismology for seismic activity prediction and seismic zoning, which can be expressed in the following form:

$$\log_{10}N(M) = -aM + b, \tag{1}$$

where M is the magnitude of the earthquake; $N(M)$ is the cumulative frequency of the earthquake; and a and b are constants. This theory reflects the relationship between the cumulative frequency and magnitude of earthquakes. The occurrence frequency of volcanic activity and its associated seismic activity have similar characteristics to that of seismic activity of earthquakes alone. Therefore, using the volcanic eruption index (VEI) to replace the M , and the volcanic activity frequency $N(VEI)$ to replace the $N(M)$, the relationship between volcanic activity frequency and volcanic eruption index can be established. Based

on Liu’s (2016) [1] prediction of the eruption scale of Changbai Mountain in the past 5000 years, the eruption index and volcanic activity frequency of Changbai Mountain can be estimated. It is thus considered that in the past 5000 years, there has been one activity with a *VEI* of 7, two activities with a *VEI* of 6, and five activities with a *VEI* of 5. Based on Equation (1), the relationship between $N(VEI)$ and *VEI* can be obtained as follows:

$$\log_{10}N(VEI) = -0.2286VEI + 1.6286, \tag{2}$$

According to Liu (2016) [1], the maximum magnitude of volcanic earthquakes is roughly equal to the *VEI*, so the relationship between the magnitude of the earthquakes associated with volcanic activity in Changbai Mountain and the $N(VEI)$ can be expressed as follows:

$$\log_{10}N(VEI) = -0.2286H + 1.6286, \tag{3}$$

where H is the magnitude of earthquakes associated with volcanic activity on Changbai Mountain.

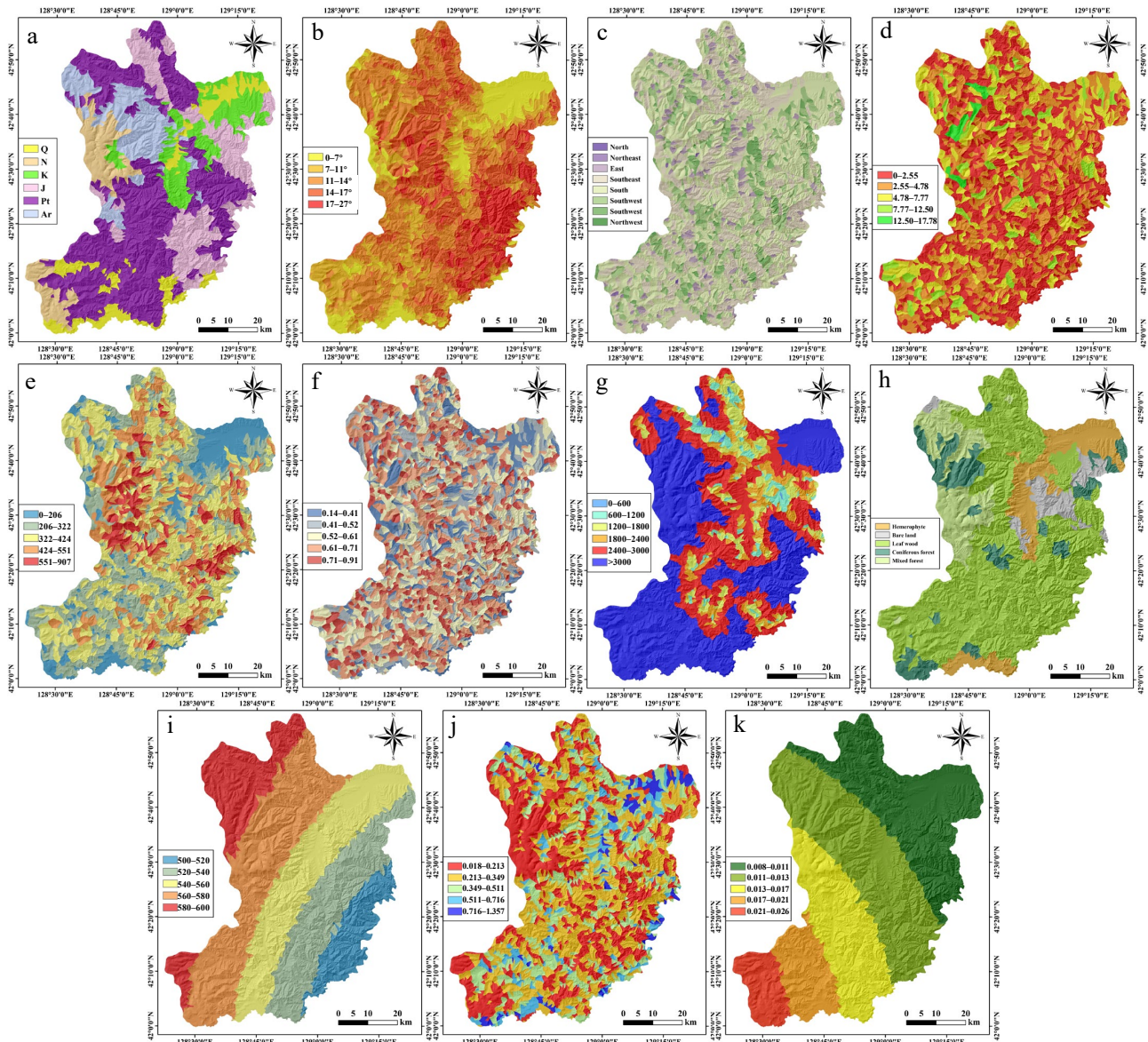


Figure 5. The conditioning factors for debris flow susceptibility mapping: (a) geology, (b) slope angle, (c) slope aspect, (d) area, (e) basin elevation difference, (f) roundness, (g) distance to fault, (h) land use, (i) average annual rainfall, (j) geomorphic information entropy, and (k) volcanic earthquake.

Table 2. Data sources and the mutator methods of each conditioning factor.

Factor	Data Source	Mutator Methods	Factor	Data Source	Mutator Methods
L ₁	Geological Survey (1:200,000)	Major	DB ₁	Geological Survey (1:200,000)	Major Actual
L ₂	DEM	Mean	DB ₂	DEM	Mean
L ₃	DEM	Mean	DB ₃	DEM	Mean
L ₄	DEM	Actual	DB ₄	DEM	Actual
L ₅	DEM	Mean	DB ₅	DEM	Actual
L ₆	Geological Survey (1:200,000)	Minimum	DB ₆	DEM	Actual
L ₇	91 Weitu software	Major	DB ₇	Geological Survey (1:200,000)	Minimum
L ₈	Statistical data (1960–2012)	Mean	DB ₈	91 Weitu software	Major
L ₉	Geological Survey (1:200,000)	Minimum	DB ₉	Statistical data (1960–2012)	Mean
L ₁₀	Geological Survey (1:200,000)	Minimum	DB ₁₀	Sun et al. (2000) [8]	Actual
L ₁₁	Chinese Ground Motion Parameter Zoning Map (GB18306–2015)	Major	DB ₁₁	Liu (2016) [1]	Minimum
L ₁₂	Liu (2016) [1]	Minimum	-	-	-

(2) Calculation of exceedance probability of earthquake intensity. There is an obvious correlation between the occurrence of geological disasters and earthquake intensity. According to statistical analysis of earthquake-induced geological disasters in various regions of China by Ding (1999) [40], it is considered that earthquake intensity VI is the minimum seismic intensity triggering geological disasters. Attenuation of earthquake intensity in eastern China can be calculated:

$$L = 1.454T - 1.792 \ln(G + 16) + 4.493, \quad (4)$$

where L is the earthquake intensity when the epicentral distance is G ; T is the magnitude; and G is the epicentral distance. Using Equation (4) can thus estimate the minimum earthquake magnitude when seismic intensity VI is reached in any place. Equation (3) can be re-arranged to obtain the annual eruption probability of Changbai Mountain volcano over 5000 years by using Equation (5):

$$P = 1/5000 \times 10^{-0.2286H+1.6286} \quad (5)$$

Combining Equations (4) and (5), the probability (P_{VI}) when seismic intensity caused by volcanic activity of Changbai Mountain exceeds VI can be calculated:

$$P_{VI} = \frac{\int_K^9 1/5000 \times 10^{-0.2286H+1.6286}}{\int_0^9 1/5000 \times 10^{-0.2286H+1.6286}}, \quad (6)$$

where K is the minimum magnitude required for the intensity to reach VI degrees. In this way, P_{VI} can be used to reflect the influence of volcanic earthquakes, which is a random event, on geological disasters in the study area.

3.3.2. Multicollinearity Analysis

The prediction accuracy of many geological hazard-susceptibility models, such as the Logistic regression model, is greatly affected by the multicollinearity of the conditioning

factors [41]. Variance inflation factor (VIF) is often used to analyze the multicollinearity of multiple conditioning factors. The calculation equation of VIF is as follows [41]:

$$\text{VIF} = \frac{1}{1 - R_i^2}, \quad (7)$$

where R_i is the complex correlation coefficient between conditioning factor X_i and other conditioning factors. If the VIF value of any conditioning factor is greater than 10 [42], it will be excluded from the models.

3.4. Geological Disaster-Susceptibility Model

3.4.1. Support Vector Machine

The Support vector machine (SVM) method is one of the most commonly used machine learning methods for susceptibility mapping of geological hazards due to it being able to solve nonlinear and high-dimensional pattern recognition problems with fewer samples than required by other methods [8]. It takes statistical learning theory as its basis. Based on various basis functions, this model converts linearly indivisible data into higher dimensional space, and finds a hyperplane in higher dimensional space to achieve linear divisibility. By this method, nonlinear problems in low-dimensional space can be analyzed and evaluated.

3.4.2. Artificial Neural Network

Artificial neural network (ANN) is the most commonly used machine learning method, which has been widely used in geological disaster-susceptibility mapping. There are several advantages of an ANN model: (a) good nonlinear mapping ability; (b) high degree of independent learning and strong adaptability; (c) strong fault tolerance; and (d) strong generalization ability [43]. The ANN model describes the nonlinear and extremely complex interaction between conditioning factors and geological disaster-susceptibility by the interaction relationship between neurons, and there is no need for complex mathematical formulas to represent the correlation between conditioning factors. The ANN model has good classification effect, especially suitable for classification of complex geological phenomena affected by various factors, and has advantages in simulating geological hazard-susceptibility mapping with complex relationships and interaction between variables.

3.5. Validation Methods

3.5.1. Receiver Operating Characteristic Curve

The receiver operating characteristic curve (ROC) is an accuracy assessment method, which is a quantitative evaluation method for the binary classification model [8]. It takes the sensitivity (false positive rate) as X-axis and 1-specificity (true positive rate) as Y-axis. The AUC value is the area under the ROC curve. For any prediction experiment, the AUC value is always in the range of 0.5 to 1. The closer the AUC value is to 1, the higher is the prediction accuracy of the model. The ROC evaluation process is simple and the evaluation results are very intuitive so that the prediction effect can be preliminarily judged only by the naked eye. Therefore, it has been widely used in the evaluation of geological hazard-susceptibility models.

3.5.2. Statistical Parameters

The validation method based on statistical parameters can verify the effectiveness of the geological hazard-susceptibility models. The statistical parameters used in this paper are shown as follows [8]:

$$\text{Accuracy(AC)} = \frac{\text{True positive} + \text{True negative}}{\text{True positive} + \text{True negative} + \text{False positive} + \text{False negative}}, \quad (8)$$

$$\text{Sensitivity(SE)} = \frac{\text{True positive}}{\text{True positive} + \text{False negative}}, \quad (9)$$

$$\text{Specificity(SP)} = \frac{\text{True negative}}{\text{True negative} + \text{False positive}}, \quad (10)$$

$$\text{Positive predictive value(PPA)} = \frac{\text{True positive}}{\text{True positive} + \text{False positive}}, \quad (11)$$

$$\text{Negative predictive value(NPV)} = \frac{\text{True negative}}{\text{True negative} + \text{False negative}}, \quad (12)$$

where true positive indicates the number of geological hazard units correctly identified; true negative represents the number of non-geological hazard units correctly identified; false positive indicates the number of geological hazard units incorrectly identified; and false negative indicates the number of non-geological hazard units incorrectly identified.

3.5.3. Cross Validation

Cross-validation can overcome the problem of insufficient data and effectively avoids the problem of over-fitting the model [9]. In this paper, the five-fold cross-validation method is adopted to verify the geological hazard-susceptibility model. It randomly divides the whole data set into five subsets, four of which are selected as the training data and the remaining one as the test data, until all five subsets are used as training data and test data, respectively. In this way, the model was trained five times and tested for five times. Then, the prediction accuracy of the model was evaluated by combining the prediction accuracy of five model runs.

3.6. The Importance of Conditioning Factors

3.6.1. Variance-Based Method

This paper uses sensitivity analysis to calculate the reduction in target variance attributable to each conditioning factor, thus determining the order of importance of each conditioning factor. The sensitivity analysis is as follows [8,44]:

$$G_i = \frac{K_i}{K(H)} = \frac{K(E(H|Y_i))}{K(H)}, \quad (13)$$

where G_i is the sensitivity; Y_i is the conditioning factor, and $i = 1, 2, \dots, k$; k is the number of the conditioning factor; H indicates whether there is landslide or not, with $H = f(Y_1, Y_2, \dots, Y_k)$ refers to modeling for H using Y_1 to Y_k ; and $K(H)$ is the unconditional output variance. Hence, the importance of each conditioning factor can be calculated by using the normalized sensitivity:

$$I_i = \frac{G_i}{\sum_{i=1}^k G_i}, \quad (14)$$

where I_i is the importance of each conditioning factor.

3.6.2. Frequency Ratio Method

The variance-based method can reflect the overall importance of the conditioning factors, while the frequency ratio (FR) can reflect the correlation between each subclass of the conditioning factors and the occurrence of geological disasters. The FR value of a subclass of a conditioning factor can be calculated as follows [45,46]:

$$FR = \frac{n/N}{m/M}, \quad (15)$$

where n represents the number of geological hazards at a particular subclass of the conditioning factor; N is the total number of the geological hazards; m represents the area of the particular subclass of the conditioning factor; and M is the total area of the study area. It

can be seen from Equation (15) that the frequency ratio reflects the possibility of occurrence and non-occurrence of geological disasters with a given attribute [7]. In the relationship analysis, an FR value of 1 means that the geological disaster density of this subclass is proportional to the size of this subclass in the conditioning factor map. Therefore, 1 is an average; an FR value greater than 1 indicates a high correlation; and a value less than 1 indicates a low correlation.

4. Results and Discussion

4.1. Multicollinearity Analysis Results

Before the multicollinearity analysis of the conditioning factors, the normalization of the conditioning factors is carried out to eliminate the influence of different dimensions. The normalization equation is as follows [41]:

$$A = \frac{A - A_{min}}{A_{max} - A_{min}}, \tag{16}$$

where A is the normalized value; A is the original value of the conditioning factors; and A_{max} and A_{min} are the maximum and minimum value of the conditioning factors, respectively. Hence, based on the principle of VIF values, the VIF values of each conditioning factors are calculated and listed in Table 3. It can be seen from Table 3 that VIF values of each conditioning factors are all less than 10, so no conditioning factors need to be moved out of the model.

Table 3. VIF value of the conditioning factors.

Factor	L ₁	L ₂	L ₃	L ₄	L ₅	L ₆	L ₇	L ₈	L ₉	L ₁₀	L ₁₁	L ₁₂
VIF	1.474	3.301	1.009	2.436	1.032	1.150	1.406	1.986	1.245	1.291	1.719	1.458
<i>p</i> -value	0.000	0.000	0.014	0.006	0.000	0.000	0.000	0.000	0.000	0.000	0.000	0.000
Factor	DB ₁	DB ₂	DB ₃	DB ₄	DB ₅	DB ₆	DB ₇	DB ₈	DB ₉	DB ₁₀	DB ₁₁	-
VIF	1.462	3.317	1.006	1.339	2.651	1.178	1.097	1.380	1.494	1.232	1.154	-
<i>p</i> -value	0.044	0.000	0.037	0.011	0.008	0.000	0.000	0.028	0.000	0.021	0.000	-

4.2. Modeling Results and Comparison

4.2.1. Modeling Results

According to the geological disaster inventory map and mapping unit division results, a total of 159 slope units have experienced landslide geological disasters, and 72 watershed units have experienced debris flow. An equal number of non-geological disaster units (72) are randomly selected to meet the requirements of modeling, which was a distance of at least 800 m from geological disaster units. Thus, based on the principle of five-fold cross-validation, the modeling data were randomly divided into five equal parts. The SVM model and ANN model are all built in the IBM SPSS software. The kernel function which is chosen has a great influence on the prediction accuracy of the SVM model. In the SVM model, the kernel function determines the radial basis function, and is affected by the C (regularization parameter) and g (kernel parameter). In this study, C is set to 0.8, and g is set to 0.5. An ANN model, which consists of an input, a hidden layer, and an output layer, was also built. The activation function determines the logistic sigmoid. The momentum, learning rate, and training time are set as 0.3, 0.3, and 500, respectively. The modeling results are listed in Table 4.

4.2.2. Landslide-Susceptibility Model Comparison

The susceptibility of typical geological hazards in the study area was modeled by the above methods. The ANN model and SVM model are compared based on the modeling results (Table 4). Table 4 shows, in the training stage, that the mean accuracy of the SVM model and the ANN model are not very different, being 0.850 and 0.831, respectively.

However, in the testing stage, the mean accuracy of the SVM (0.824) is much higher than that of the ANN (0.728) model. From the standard deviation of mean accuracy, it can be seen that in both training and testing stages, the stability of the SVM model is better than the ANN model: Training stage: 0.005 for SVM model and 0.034 for ANN model; Testing stage: 0.044 for SVM model and 0.053 for ANN model. Thus, on the basis specifically of mean accuracy, SVM model is significantly better than ANN model. Based on the other four statistical parameters, the standard deviation of the SVM model is generally smaller than that of the ANN model, which shows that the SVM model is superior to the ANN model in terms of stability. In the training stage, based on the mean value of the four parameters, the SVM model is not much different to the ANN model; however, in the testing stage, the mean values of the four parameters of the SVM model are generally greater than those of the ANN model. The mean value and stability of the five statistical parameters of the two models both decreased during the testing stage, and the ANN model decreased greatly. In addition, based on the AUC value, the SVM (0.895) model is not much different than that of the ANN (0.910) model in the training stage; the SVM (0.873) model is higher than that of the ANN (0.832) model in the testing stage. In conclusion, on the basis of statistical parameters and the AUC value, the SVM model is superior to the ANN model.

Table 4. The modeling results of the SVM model and ANN models.

Method	Index	Training							Validating						
		K = 1	K = 2	K = 3	K = 4	K = 5	Mean	Standard Deviation	K = 1	K = 2	K = 3	K = 4	K = 5	Mean	Standard Deviation
Landslide susceptibility model															
SVM	AC	0.849	0.846	0.848	0.850	0.858	0.850	0.005	0.875	0.859	0.806	0.813	0.766	0.824	0.044
	SE	0.858	0.849	0.845	0.856	0.870	0.856	0.010	0.875	0.848	0.880	0.889	0.774	0.853	0.047
	SP	0.821	0.844	0.850	0.845	0.847	0.841	0.012	0.875	0.871	0.757	0.857	0.758	0.823	0.061
	PPV	0.811	0.843	0.852	0.843	0.843	0.838	0.016	0.875	0.875	0.710	0.875	0.750	0.817	0.081
	NPV	0.866	0.850	0.844	0.858	0.874	0.859	0.012	0.875	0.844	0.903	0.750	0.781	0.831	0.064
	AUC	0.902	0.898	0.914	0.906	0.853	0.895	0.024	0.926	0.897	0.829	0.891	0.828	0.874	0.044
ANN	AC	0.811	0.839	0.840	0.787	0.878	0.831	0.034	0.719	0.844	0.774	0.734	0.719	0.758	0.053
	SE	0.811	0.877	0.848	0.817	0.881	0.847	0.033	0.719	0.844	0.815	0.703	0.733	0.763	0.063
	SP	0.811	0.807	0.832	0.763	0.875	0.818	0.041	0.719	0.844	0.743	0.778	0.706	0.758	0.055
	PPV	0.811	0.787	0.828	0.740	0.874	0.808	0.049	0.719	0.844	0.710	0.813	0.688	0.754	0.069
	NPV	0.811	0.890	0.852	0.835	0.882	0.854	0.033	0.719	0.844	0.839	0.656	0.750	0.761	0.080
	AUC	0.881	0.914	0.930	0.880	0.943	0.910	0.028	0.811	0.883	0.842	0.848	0.775	0.832	0.041
Debris flow susceptibility model															
SVM	AC	0.810	0.810	0.793	0.798	0.798	0.802	0.008	0.679	0.643	0.786	0.767	0.767	0.728	0.063
	SE	0.833	0.833	0.815	0.815	0.815	0.822	0.010	0.667	0.667	0.900	0.722	0.786	0.748	0.098
	SP	0.790	0.790	0.774	0.783	0.783	0.784	0.007	0.692	0.625	0.722	0.833	0.750	0.725	0.077
	PPV	0.776	0.776	0.759	0.772	0.772	0.771	0.007	0.714	0.571	0.643	0.867	0.733	0.706	0.110
	NPV	0.845	0.845	0.828	0.825	0.825	0.833	0.011	0.643	0.714	0.929	0.667	0.800	0.750	0.116
	AUC	0.883	0.868	0.880	0.861	0.870	0.872	0.009	0.770	0.786	0.806	0.929	0.853	0.829	0.064
ANN	AC	0.784	0.767	0.793	0.798	0.728	0.774	0.028	0.643	0.679	0.786	0.667	0.733	0.701	0.058
	SE	0.789	0.731	0.854	0.774	0.710	0.772	0.056	0.625	0.692	0.900	0.619	0.769	0.721	0.117
	SP	0.780	0.816	0.750	0.827	0.750	0.785	0.036	0.667	0.667	0.722	0.778	0.706	0.708	0.046
	PPV	0.776	0.845	0.707	0.842	0.772	0.788	0.057	0.714	0.643	0.643	0.867	0.667	0.707	0.094
	NPV	0.793	0.690	0.879	0.754	0.684	0.760	0.081	0.571	0.714	0.929	0.467	0.800	0.696	0.183
	AUC	0.917	0.850	0.926	0.881	0.849	0.885	0.036	0.786	0.847	0.765	0.893	0.747	0.808	0.061

4.2.3. Debris Flow Susceptibility Model Comparison

From Table 4, it can be seen that, in the training stage, the mean accuracy of the SVM (0.802) model is higher than that of the ANN (0.774) model; the SVM (0.728) model is also higher than that of the ANN (0.701) model in the testing stage. For the standard deviation of mean accuracy, the standard deviation of the SVM (0.008) model was smaller in the training stage, while the standard deviation of the ANN (0.028) model was larger; in the testing stage, the accuracy standard deviation of the SVM (0.063) model and the ANN (0.058) model both increased, while the SVM model increased more significantly. The two models were evaluated based on accuracy only. The mean accuracy and standard deviation of the two models decreased in the testing stage compared with the training stage, but the decrease was not significant, and the standard deviation of accuracy was below 0.07. Therefore, the SVM model was considered the optimal model. For the other four statistical parameters, their standard deviations were all small for the SVM model in

the training stage, while for the ANN model they were all large, indicating that the stability of the two models had decreased. The standard deviations of the four statistical parameters increased significantly in the testing stage compared with the training stage. This shows that the stability of these two models is worse in the testing stage than in the training stage. The mean values of the four statistical parameters for the SVM model are significantly higher than for the ANN model in both training and testing stages. Moreover, the AUC value for the SVM (0.872) model is not much different to that of the ANN (0.885) model in the training stage; and in the testing stage, it is higher for the SVM (0.829) model than for the ANN (0.808) model. In conclusion, from the perspective of statistical parameters and the AUC value, the SVM model is superior to the ANN model.

4.2.4. Comparison with Other Models

Some similar research studies are being carried out in Helong city. Based on the ICM method (information content method) and the AHP method (analytic hierarchy process), Yu and Chen (2020) [23] analyzed the landslide susceptibility of Helong city by using the slope unit and grid unit. According to the frequency ratio (FR), Yu (2021) [47] assessed the debris flow susceptibility of Helong city by using the watershed unit. From Table 5, it can be seen that the landslide susceptibility model established using the slope unit is superior to that established using the grid unit, since the slope unit is more consistent with the real terrain. Moreover, the prediction accuracy of the landslide susceptibility model and debris flow susceptibility model established in this study is higher than that of Yu and Chen (2020) [23] and Yu (2021) [47], which indicates that the geological hazard-susceptibility model in this present study is suitable for predicting the susceptibility of geological hazards in the study area.

Table 5. Model fitting results of the study area.

Source	Type	Mapping Units	Method	AUC (Mean)
This study		Slope units	SVM	89.5% (Training)/87.4% (Testing)
			ANN	91.0% (Training)/83.2% (Testing)
Yu and Chen (2020) [23]	Landslide Susceptibility mapping	Grid units	ICM	83.4%
			AHP	70.9%
		Slope units	ICM	87.1%
			AHP	80.5%
This study	Debris flow susceptibility mapping	Watershed units	ANN	87.2% (Training)/82.9% (Testing)
			SVM	88.5% (Training)/80.8% (Testing)
Yu (2021) [47]			FR	85.3%

Note: SVM = support vector machine; ANN = artificial neural network; ICM = information content method; AHP = analytic hierarchy process; FR= frequency ratio.

4.3. Analysis of Importance of Conditioning Factors

4.3.1. Analysis of Importance of Landslide Conditioning Factors

According to the variance-based method, the importance of each landslide conditioning factors under the five-fold cross-validation of the SVM model and ANN model was determined. The mean importance index is used to reflect the influence degree of each conditioning factor on the occurrence and spatial distribution of landslide (Figure 6). It can be seen that the L_9 (distance to river) is the most important conditioning factor for landslide susceptibility modeling (0.396 for SVM model, and 0.096 for ANN model). From the relationship between FR value and L_9 (Table 6), the FR value of each subclass presents a downward trend with the increase in river distance. This is because the slope foot has suffered from the river erosion for a long time. The material at the foot of the slope will gradually loosen, and then be carried and transported away by the river, leading to the

slope angle gradually becoming steeper. In adapting to the erosion of the river, the slope angle often decreases rapidly by way of landslide. Moreover, from the FR value (2.11 for slope angle class 18–24°, and 29.06 for slope angle class 24–30°), it can also be seen that the steeper the slope angle (L_2), the more prone it is to landslide. Secondly, the strength at the foot of slopes suffering from river immersion will gradually reduce, forming a geological environment conducive to the occurrence of landslide disasters. In general, the closer a river is, the more intense is the river erosion.

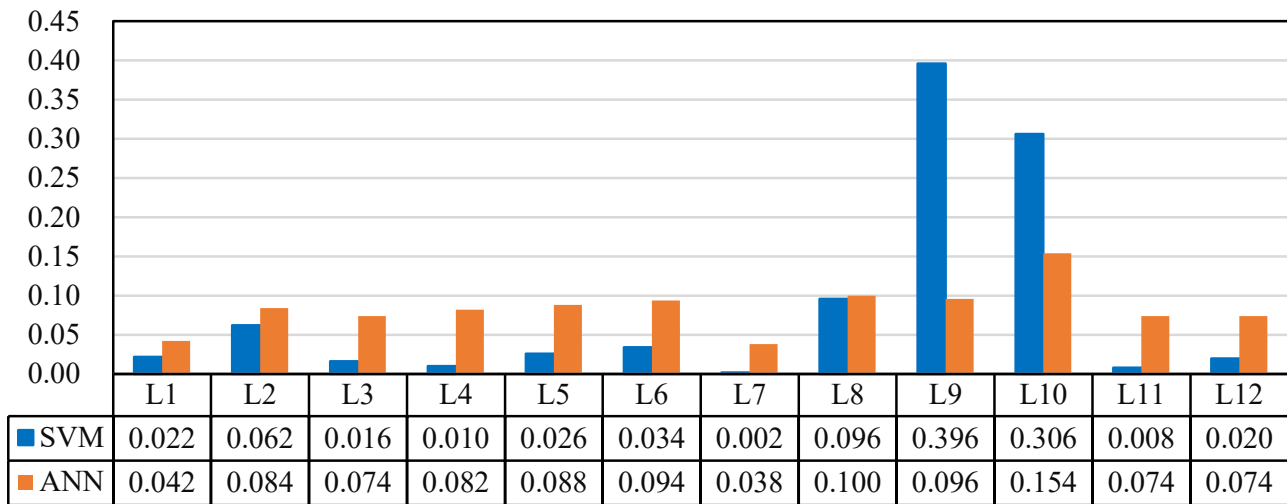


Figure 6. Importance of landslide conditioning factors to the SVM and ANN models.

Table 6. Statistics of FR values of each subclass of the landslide conditioning factors.

Factors	Class	FR	Factors	Class	FR	Factors	Class	FR	
L ₁	Q	1.72	L ₄	180–252	0.78	L ₈	580–600	0.12	
	N	0.10		252–339	1.30		0–500	3.11	
	K	0.58		339–595	1.03		500–1000	1.00	
	L ₂	J	1.80	L ₅	Concave	1.27	L ₉	1000–1500	0.53
		Pt	0.97		Flat	0.57		1500–2000	0.51
		Ar	0.73		Convex	1.68		2000–2500	0.70
L ₃	0–6	0.27	L ₆	0–600	1.14	L ₁₀	>2500	0.46	
	6–12	0.85		600–1200	0.82		0–500	2.66	
	12–18	0.96		1200–1800	1.35		500–1000	2.99	
	18–24	2.11		1800–2400	1.03		1000–1500	1.45	
	24–30	29.06		2400–3000	1.17		1500–2000	0.72	
L ₄	N	0.00	L ₇	>3000	0.92	L ₁₁	2000–2500	0.13	
	NE	0.20		Hemerophyte	1.59		>2500	0.50	
	E	0.88		Bare land	1.74		VI	1.12	
	SE	1.20		Leaf wood	1.21		VII	0.22	
	L ₅	S	1.53	Coniferous forest	0.31	L ₁₂	VIII	0.00	
		SW	0.88	Mixed forest	0.09		0.008–0.011	1.16	
		W	0.52	500–520	3.76		0.011–0.013	1.19	
		NW	0.32	520–540	0.92		0.013–0.016	0.98	
L ₆	0–103	0.74	L ₈	540–560	0.68	0.016–0.020	0.56		
	103–180	1.19		560–580	0.27	0.020–0.026	0.09		

The L_{10} (distance to road) is another important conditioning factor (0.306 for SVM model, and 0.154 for ANN model). Based on the field survey, more than 80% of landslide disasters in the study area are caused by human engineering activities, among which the excavation of highways is the most frequent factor. This destroys the originally stable natural slope angle, forms a free face or steep cliff, and exposes the rock mass to stronger external dynamic action, thus contributing to the topographic and geomorphic conditions of landslides. From the perspective of FR value, the most favorable road distance for landslide occurrence is 0–1500 m.

The L_8 (average annual rainfall) is also an important factor inducing landslide in the study area (0.096 for SVM model, and 0.100 for ANN model). However, it can be seen from the FR value that with the increase of rainfall, the FR value decreases, which differs from the common understanding that the higher the rainfall intensity, the more likely landslides occur. According to statistics, the landslides that have occurred in Helong city are mostly induced by heavy rainfall. Comparing precipitation of less than 470 mm and greater than 470 mm, respectively, the number of landslides nearly doubled, especially under continuous heavy rainfall, and the flood season of every year is the season with high occurrence of landslides. However, most regions with precipitation greater than 520 mm are densely forested mountains (L_6) and human activities are rare, so there is a poor correlation between annual rainfall and landslide geological disasters.

Moreover, according to Table 6 and the field investigation results, it can be determined that the most favorable combination of geological conditions for landslide occurrence in the study area is as follows: Q , K and J for L_1 ; $18\text{--}30^\circ$ for L_2 ; SE, and S for L_3 ; 103–180 m, 252–339 m, 339–595 m for L_4 ; convex for L_5 ; distance to L_6 within 3000 m; hemerophyte, bare land, leaf wood for L_7 ; L_8 greater than 470 mm; distance to L_9 within 1000 m; distance to L_{10} within 1500 m; and the larger L_{11} and L_{12} .

4.3.2. Analysis of Importance of Debris Flow Conditioning Factors

From Figure 7, it can be seen that the DB_2 (slope angle) is the most important conditioning factor for debris flow susceptibility model (0.298 for SVM model, and 0.138 for ANN model). According to the field investigation results, there are many gully debris flows along the roads of Helong City, while hill and mountain areas most commonly present hillside debris flows. Gully debris flow is distributed in valleys with large slope and rich debris material, while hillside debris flow is generally distributed in gullies with large longitudinal slope and a large proportion of recharge section. From the relationship between FR value and DB_2 (Table 7), the development degree of debris flow can be seen to decrease with the increase in slope angle. This is because 60 debris flows in Helong city are of gully type, with large catchment area and gentle terrain slope compared with hillside type, so there are more debris flows with smaller slope. The DB_{11} (volcanic earthquake) is the second most important conditioning factor (0.204 for SVM model, and 0.168 for ANN model). Geological disasters such as landslide induced by volcanic earthquake can provide rich material sources for the occurrence of debris flow. The DB_8 (land use) is also an important conditioning factor for debris flow occurrence (0.168 for SVM model, and 0.084 for ANN model). In terms of FR value, the land use with high correlation for debris flow occurrence is bare land (1.89) and hemerophyte (3.76). The results show that debris flow is more likely to occur in hemerophyte and bare land due to the low vegetation coverage and the loss of vegetation protection.

Debris flow is prone to occur in areas with large topographic fluctuations, and steep terrain endows the provenance in the basin with a large potential energy. Once stimulated by rainfall with sufficient intensity, debris flow is likely to form in the basin. As a parameter reflecting the degree of topographic relief and the development stage of watershed, geomorphic information entropy (DB_{10}) can reflect the complexity of the terrain in the valley. According to the FR value, the subclass 0.349–1.357 of DB_{10} is most conducive to the occurrence of debris flow. Based on the geomorphic development stage reflected by the DB_{10} value, debris flow gullies in the study area are in the prime- to old-age stage, indicating

that these gullies are in the stage of intense erosion, have the provenance conditions of debris flow, and are very likely to present debris flow.

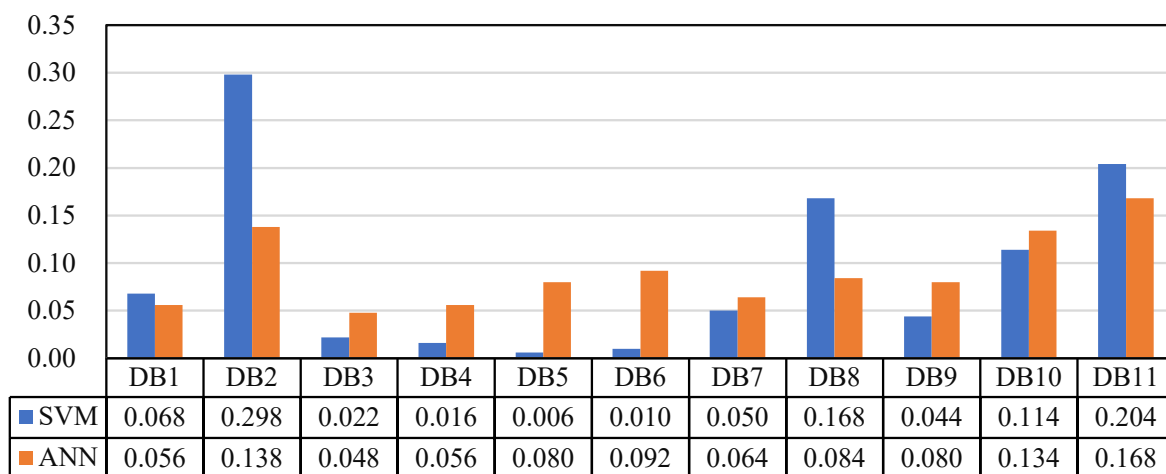


Figure 7. Importance of debris flow conditioning factors for the SVM and ANN models.

Table 7. Statistics of FR values of each subclass of the debris flow conditioning factors.

Factors	Class	FR	Factors	Class	FR	Factors	Class	FR
DB ₁	Q	1.79	DB ₄	2.55–4.78	1.17	DB ₈	Hemerophyte	3.76
	N	0.00		4.78–7.77	1.15		Bare land	1.89
	K	4.63		7.77–12.50	0.90		Leaf wood	0.63
	J	1.37		12.50–17.78	0.00	Coniferous forest	0.39	
	Pt	0.16	DB ₅	0–206	3.38	Mixed forest	0.00	
	Ar	0.60		206–322	0.67	500–520	0.45	
DB ₂	0–7	3.48	DB ₅	322–424	0.73	DB ₉	520–540	0.90
	7–11	1.50		424–551	0.70		540–560	2.61
	11–14	0.26		551–907	0.56		560–580	0.41
	14–17	0.71		DB ₆	0.14–0.41		1.75	580–600
	17–27	0.42	0.41–0.52		1.50	0.018–0.213	0.34	
DB ₃	N	0.00	DB ₆	0.52–0.61	0.95	DB ₁₀	0.213–0.349	0.83
	NE	0.00		0.61–0.71	0.77		0.349–0.511	1.53
	E	1.81		0.71–0.91	0.34		0.511–0.716	2.32
	SE	0.59	DB ₇	0–600	0.87	0.716–1.357	3.25	
	S	1.17		600–1200	1.42	0.008–0.011	2.38	
	SW	1.11		1200–1800	1.62	0.011–0.013	0.85	
	W	0.89		1800–2400	1.07	0.013–0.017	0.00	
NW	0.00	2400–3000	0.00	DB ₁₁	0.017–0.021	0.00		
DB ₄	0–2.55	0.86	>3000		0.92	0.021–0.026	0.00	

In summary, according to Table 7 and the field investigation results, it can be determined that the most favorable combination of geological conditions for debris flow occurrence in the study area is as follows: Q, K and J for DB₁; 6–11° for DB₂; E, S, and SE for DB₃; 1.55–7.77 km² for DB₄; 0–206 m for DB₅; 0.14–0.52 for L₆; distance to DB₇ within 2400 m; hemerophyte, bare land for DB₈; DB₉ greater than 470 mm; 0.349–1.357 for DB₁₀; the larger DB₁₁.

4.4. Geological Hazard-Susceptibility Map Analysis

Based on the susceptibility model results of landslide and debris flow, and the comparison of the two models, it is determined that the best model for susceptibility mapping of both geological disasters is the SVM model. Therefore, this paper finally adopts the SVM model for mapping of landslide and debris flow susceptibility in the study area. The susceptibility map was produced by using the model with highest accuracy in the modeling process. The susceptibility of geological disasters is classified into four grades: low, moderate, high, and very high, by using the natural breaks method. The final landslide and debris flow susceptibility mapping maps are shown in Figure 8.

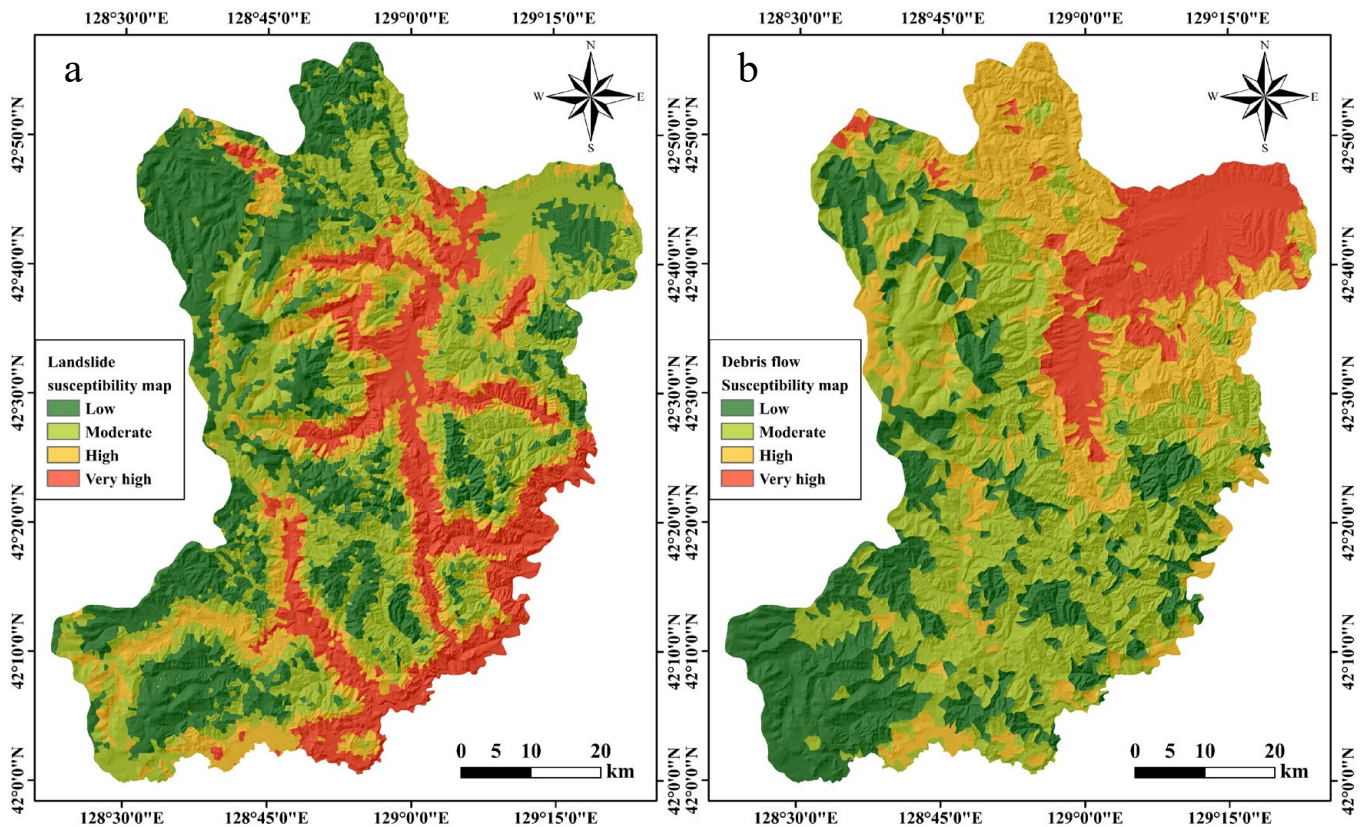


Figure 8. Geological hazard-susceptibility map: (a) landslide susceptibility map, (b) debris flow susceptibility map.

Based on the geological hazard-susceptibility map's statistical data (Table 8), the areas with low, moderate, high, and very high landslide susceptibility are 1299.28, 1935.73, 1189.63, and 643.98 km², accounting for 31.58%, 33.15%, 17.07%, and 18.19% of the total study area, respectively. The landslide numbers included in the four landslide susceptibility areas are 3, 20, 14, and 122, respectively, accounting for 1.89%, 12.58%, 8.81%, and 76.73% of the total landslides, respectively. The areas with low, moderate, high, and very high debris flow susceptibility are 1600.98, 1680.37, 865.12, and 922.15 km², respectively, accounting for 25.63%, 38.19%, 23.47%, and 12.71% of the total study area, respectively. The debris flow number included in the four landslide susceptibility areas are 1, 13, 7, and 51, respectively, accounting for 1.39%, 18.06%, 9.72%, and 70.83% of the total debris flows, respectively. According to the statistical data, the areas with very high and high landslide susceptibility and debris flow susceptibility account for 35.26% and 36.18%, respectively. However, these actually account for 85.54% of the known landslides and 80.55% of the known debris flows, respectively, which shows that the geological hazard-susceptibility maps in this study are reasonable.

Table 8. Statistical results of the geological hazard-susceptibility maps.

Type	Susceptibility	Geological Hazard Occurred Number	Ratio	Total Study Area Area(km ²)	Ratio
Landslide susceptibility map	Low	3	1.89%	1299.28	31.58%
	Moderate	20	12.58%	1935.73	33.15%
	High	14	8.81%	1189.63	17.07%
	Very High	122	76.73%	643.98	18.19%
Debris flow susceptibility map	Low	1	1.39%	1600.98	25.63%
	Moderate	13	18.06%	1680.37	38.19%
	High	7	9.72%	865.12	23.47%
	Very High	51	70.83%	922.15	12.71%

From Figure 8a, it is seen that the areas with low and moderate susceptibility are distributed in the area with high elevation, accounting for 64.73% of the study area. In this area, the vegetation is mainly coniferous forest, broadleaved forest, and mixed coniferous–broadleaved forest, and the vegetation coverage rate is high. Moreover, this area is far from the main rivers and faults in the study area, and the erosion of rivers and tectonic activities of faults have little influence. Due to the influence of elevation, human engineering activities in this area are also very small, so the risk of landslide geological disaster in this area is relatively low. Where the landslide susceptibility grade is from high to very high, this is mainly in the lower elevation area, accounting for 35.26% of the area. Here, human engineering activities are extremely intense, such as road excavation and urban expansion, which have a great impact on the stability of the slope body. Furthermore, from the perspective of geological environment, this region is mainly bare land and artificial vegetation, with a low vegetation coverage rate and relatively close distance from rivers, roads, and faults. It is strongly affected by human engineering activities, river action, and geological tectonic activities. Therefore, the risk of landslide geological disaster in this region is relatively high. It can also be seen (Figure 8a) that the susceptibility of landslide geological disaster is low to moderate in areas far from the main areas of human production and living activities, thus causing relatively little harm when landslide geological disaster occurs. The areas with high to very high landslide susceptibility are mainly distributed around the towns where human life and production activities are concentrated. In these regions, population density, building density, cultivated land density is high, and the level of industrialization is relatively developed: therefore, once landslide occurs, serious loss of life and property will be caused. Therefore, it is suggested to strengthen disaster monitoring in these areas, realize real-time monitoring and early warning of landslide disasters, and pay attention to the deployment of disaster prevention and mitigation.

From Figure 8b, it can be seen that the area with low to moderate susceptibility of debris flow in Helong city accounts for 63.82%, which indicates that the risk of debris flow in Helong City is generally low. This area is also distributed in the relatively high elevation of the study area, with high vegetation coverage and little influence from human engineering activities, fluvial action, and tectonism. The areas of high to very high susceptibility of debris flow in Helong city, accounting for 36.18% of the study area, are mainly distributed in the lower elevation area, and mainly distributed in the northeast of Longcheng Town, Bajiazi Town, the middle of Toudao Town, and the north part of Dongcheng Town. These have a high population density and are greatly affected by human engineering activities. The vegetation coverage rate here is extremely low, and bare land and artificial vegetation are the most common land-use types. Once the geological disaster of debris flow breaks out in any of these areas, it will cause great economic and property losses to the towns mentioned above. Therefore, it is suggested to strengthen the monitoring and early warning research of debris flow disasters in these areas, and realize the early warning of debris flow geological disaster through monitoring rainfall and so on, to reduce the degree of danger of debris flow disaster.

5. Conclusions

In this study, geological hazard-susceptibility mapping, including landslide and debris flow susceptibility mapping, was carried out in Helong city. This study selected the slope unit and watershed unit as the mapping units. The transcendental probability of Changbai Mountain volcanic earthquake greater than VI degrees was used to indicate the relationship between the geological hazard-susceptibility and Changbai Mountain volcanic earthquake. Eleven other landslide conditioning factors were also selected as the evaluation factors, namely the (a) geology, (b) slope angle, (c) slope aspect, (d) topographic relief, (e) curvature, (f) distance to fault, (g) land use, (h) average annual rainfall, (i) distance to river, (j) road distance, (k) basic earthquake intensity, and (l) volcanic earthquake; along with ten other debris flow conditioning factors, namely (a) geology, (b) slope angle, (c) slope aspect, (d) area, (e) basin elevation difference, (f) roundness, (g) distance to fault, (h) land use, (i) average annual rainfall, and (j) geomorphic information entropy. Two models, an SVM model and an ANN model, were then compared and evaluated. The following inferences were obtained:

- (1) According to the modeling results, the SVM model is better than the ANN model for both the landslide susceptibility mapping and debris flow susceptibility mapping. The landslide susceptibility map modeled by the SVM model shows that the areas with low, moderate, high, and very high landslide susceptibility are 31.58%, 33.15%, 17.07%, and 18.19% of the total study area, respectively. Moreover, the high and very high landslide susceptibility classes make up 85.54% of the known landslides. The areas with low, moderate, high, and very high debris flow susceptibility are 25.63%, 38.19%, 23.47%, and 12.71% of the total study area, respectively, with high and very high debris flow susceptibility classes accounting for 80.55% of the known debris flows.
- (2) Distance to river, distance to road, and average annual rainfall were the three most significant factors for landslide susceptibility mapping; and slope angle, volcanic earthquake, land use, and geomorphic information entropy were the four most significant factors for debris flow susceptibility mapping.
- (3) From the landslide susceptibility and debris flows susceptibility map results, it can be seen that the very high and high landslide and debris flow susceptibility are mainly distributed in areas of lower elevation, and mainly distributed around the cities and towns in Helong City. Thus, it is suggested to strengthen disaster monitoring in these areas, realize real-time monitoring and early warning of geological disasters, and pay attention to the deployment of disaster prevention and mitigation.

Author Contributions: Writing—original draft preparation, methodology, formal analysis, and validation Xiaohui Sun and Chenglong Yu; writing—review and editing, Yanrong Li and Ngambua N. Rene. All authors have read and agreed to the published version of the manuscript.

Funding: This research received no external funding.

Data Availability Statement: Not applicable.

Acknowledgments: The authors would like to thank the editor and anonymous reviewers for their comments and suggestions which helped significantly improve this paper.

Conflicts of Interest: The authors declare no conflict of interest.

References

1. Liu, X. Hazard Assessment of Landslide and Collapse Induced by Volcanic Eruption in Changbai Mountains. Master's Thesis, Jilin University, Changchun, China, 2016.
2. Liu, G.S.H.; Guo, F. The newest monitoring information of Changbaishan volcano, NE China. *Acta Petrol. Sin.* **2011**, *27*, 2905–2911.
3. Blais-Stevens, A.; Behnia, P.; Kremer, M.; Page, A.; Kung, R.; Bonham-Carter, G. Landslide susceptibility mapping of the Sea to Sky transportation corridor, British Columbia, Canada: Comparison of two methods. *Bull. Eng. Geol. Environ.* **2012**, *71*, 447–466. [[CrossRef](#)]

4. Kayastha, P.; Dhital, M.R.; De Smedt, F. Evaluation and comparison of GIS based landslide susceptibility mapping procedures in Kulekhani watershed, Nepal. *J. Geol. Soc. India* **2013**, *81*, 219–231. [[CrossRef](#)]
5. Van Westen, C.J.; Rengers, N.; Soeters, R. Use of geomorphological information in indirect landslide susceptibility assessment. *Nat. Hazards* **2003**, *30*, 399–419. [[CrossRef](#)]
6. Steger, S.; Bell, R.; Petschko, H.; Glade, T. Evaluating the Effect of Modelling Methods and Landslide Inventories Used for Statistical Susceptibility Modelling. In Proceedings of the 12th International IAEG Congress, Torino, Italy, 15–19 September 2015; pp. 201–204.
7. Sun, X.; Chen, J.; Bao, Y.; Han, X.; Zhan, J.; Peng, W. Landslide Susceptibility Mapping Using Logistic Regression Analysis along the Jinsha River and Its Tributaries Close to Derong and Deqin County, Southwestern China. *Isprs Int. J. Geo-Inf.* **2018**, *7*, 438. [[CrossRef](#)]
8. Sun, X.; Chen, J.; Han, X.; Bao, Y.; Zhan, J.; Peng, W. Application of a GIS-based slope unit method for landslide susceptibility mapping along the rapidly uplifting section of the upper Jinsha River, South-Western China. *Bull. Eng. Geol. Environ.* **2020**, *79*, 533–549. [[CrossRef](#)]
9. Sun, X.; Chen, J.; Han, X.; Bao, Y.; Zhou, X.; Peng, W. Landslide susceptibility mapping along the upper Jinsha River, south-western China: A comparison of hydrological and curvature watershed methods for slope unit classification. *Bull. Eng. Geol. Environ.* **2020**, *79*, 4657–4670. [[CrossRef](#)]
10. Leventhal, A.R.; Kotze, G.P. Landslide susceptibility and hazard mapping in Australia for land-use planning—With reference to challenges in metropolitan suburbia. *Eng. Geol.* **2008**, *102*, 238–250. [[CrossRef](#)]
11. Segoni, S.; Tofani, V.; Rosi, A.; Catani, F.; Casagli, N. Combination of Rainfall Thresholds and Susceptibility Maps for Dynamic Landslide Hazard Assessment at Regional Scale. *Front. Earth Sci.* **2018**, *6*, 85. [[CrossRef](#)]
12. Shit, P.K.; Bhunia, G.S.; Maiti, R. Potential landslide susceptibility mapping using weighted overlay model (WOM). *Modeling Earth Syst. Environ.* **2016**, *2*, 21. [[CrossRef](#)]
13. Farahani, S.; Behnam, B.; Tahershamsi, A. Macrozonation of seismic transient and permanent ground deformation of Iran. *Nat. Hazards Earth Syst. Sci.* **2020**, *20*, 2889–2903. [[CrossRef](#)]
14. Farahani, S.; Tahershamsi, A.; Behnam, B. Earthquake and post-earthquake vulnerability assessment of urban gas pipelines network. *Nat. Hazards* **2020**, *101*, 327–347. [[CrossRef](#)]
15. Binita, K.C.; Shepherd, J.M.; King, A.W.; Johnson Gaither, C. Multi-hazard climate risk projections for the United States. *Nat. Hazards* **2021**, *105*, 1963–1976. [[CrossRef](#)]
16. Guzzetti, F.; Mondini, A.C.; Cardinali, M.; Fiorucci, F.; Santangelo, M.; Chang, K.-T. Landslide inventory maps: New tools for an old problem. *Earth-Sci. Rev.* **2012**, *112*, 42–66. [[CrossRef](#)]
17. Dai, K.; Li, Z.; Tomas, R.; Liu, G.; Yu, B.; Wang, X.; Cheng, H.; Chen, J.; Stockamp, J. Monitoring activity at the Daguangbao mega-landslide (China) using Sentinel-1 TOPS time series interferometry. *Remote Sens. Environ.* **2016**, *186*, 501–513. [[CrossRef](#)]
18. Zhao, C.; Kang, Y.; Zhang, Q.; Zhu, W.; Li, B.; IEEE. Landslide detection and monitoring with insar technique over upper reaches of jinsha river, China. In Proceedings of the 36th IEEE International Geoscience and Remote Sensing Symposium (IGARSS), Beijing, China, 10–15 July 2016; pp. 2881–2884.
19. Farova, K.; Jelenek, J.; Kopackova-Strnadova, V.; Kycl, P. Comparing DInSAR and PSI Techniques Employed to Sentinel-1 Data to Monitor Highway Stability: A Case Study of a Massive Dobkoviky Landslide, Czech Republic. *Remote Sens.* **2019**, *11*, 2670. [[CrossRef](#)]
20. Sun, X.; Chen, J.; Li, Y.; Rene, N.N. Landslide Susceptibility Mapping along a Rapidly Uplifting River Valley of the Upper Jinsha River, Southeastern Tibetan Plateau, China. *Remote Sens.* **2022**, *14*, 1730. [[CrossRef](#)]
21. Wang, F.; Xu, P.; Wang, C.; Wang, N.; Jiang, N. Application of a GIS-Based Slope Unit Method for Landslide Susceptibility Mapping along the Longzi River, Southeastern Tibetan Plateau, China. *Isprs Int. J. Geo-Inf.* **2017**, *6*, 172. [[CrossRef](#)]
22. Pourghasemi, H.R.; Rossi, M. Landslide susceptibility modeling in a landslide prone area in Mazandarn Province, north of Iran: A comparison between GLM, GAM, MARS, and M-AHP methods. *Theor. Appl. Climatol.* **2017**, *130*, 609–633. [[CrossRef](#)]
23. Yu, C.; Chen, J. Application of a GIS-Based Slope Unit Method for Landslide Susceptibility Mapping in Helong City: Comparative Assessment of ICM, AHP, and RF Model. *Symmetry-Basel* **2020**, *12*, 1848. [[CrossRef](#)]
24. Khodadad, S.; Jang, D.-H. Landslide susceptibility mapping in the Penang Island, Malaysia—Using the AHP and OLS methods. *J. Korean Geomorphol. Assoc.* **2015**, *22*, 109–121. [[CrossRef](#)]
25. Quan, H.; Deug, M.H.; Jin, G.; Park, S.-S. Landslide Susceptibility Analysis in Baekdu Mountain Area Using ANN and AHP Method. *J. Korean Geoenviron. Soc.* **2014**, *15*, 79–85. [[CrossRef](#)]
26. Wen, H.; Xie, P.; Xiao, P.; Hu, D. Rapid susceptibility mapping of earthquake-triggered slope geohazards in Lushan County by combining remote sensing with the AHP model developed for the Wenchuan earthquake. *Bull. Eng. Geol. Environ.* **2017**, *76*, 909–921. [[CrossRef](#)]
27. Hasekiogullari, G.D.; Ercanoglu, M. A new approach to use AHP in landslide susceptibility mapping: A case study at Yenice (Karabuk, NW Turkey). *Nat. Hazards* **2012**, *63*, 1157–1179. [[CrossRef](#)]
28. Kumar, S.; Snehmani, S.; Srivastava, P.K.; Gore, A.; Singh, M.K. Fuzzy-frequency ratio model for avalanche susceptibility mapping. *Int. J. Digit. Earth* **2016**, *9*, 1168–1184. [[CrossRef](#)]
29. Rabby, Y.W.; Li, Y. Landslide Susceptibility Mapping Using Integrated Methods: A Case Study in the Chittagong Hilly Areas, Bangladesh. *Geosciences* **2020**, *10*, 483. [[CrossRef](#)]

30. Yoo, Y.; Tae-Kyung, B.; Kim, J.; Park, S. A Comparative Study of the Frequency Ratio and Evidential Belief Function Models for Landslide Susceptibility Mapping. *J. Korean Soc. Surv. Geod. Photogramm. Cartogr.* **2016**, *34*, 597–607. [[CrossRef](#)]
31. Chen, W.; Li, W.; Chai, H.; Hou, E.; Li, X.; Ding, X. GIS-based landslide susceptibility mapping using analytical hierarchy process (AHP) and certainty factor (CF) models for the Baozhong region of Baoji City, China. *Environ. Earth Sci.* **2016**, *75*, 63. [[CrossRef](#)]
32. Wang, Q.; Guo, Y.; Li, W.; He, J.; Wu, Z. Predictive modeling of landslide hazards in Wen County, northwestern China based on information value, weights-of-evidence, and certainty factor. *Geomat. Nat. Hazards Risk* **2019**, *10*, 820–835. [[CrossRef](#)]
33. Chen, W.; Li, W.; Hou, E.; Bai, H.; Chai, H.; Wang, D.; Cui, X.; Wang, Q. Application of frequency ratio, statistical index, and index of entropy models and their comparison in landslide susceptibility mapping for the Baozhong Region of Baoji, China. *Arab. J. Geosci.* **2015**, *8*, 1829–1841. [[CrossRef](#)]
34. Wu, Y.; Li, W.; Wang, Q.; Liu, Q.; Yang, D.; Xing, M.; Pei, Y.; Yan, S. Landslide susceptibility assessment using frequency ratio, statistical index and certainty factor models for the Gangu County, China. *Arab. J. Geosci.* **2016**, *9*, 84. [[CrossRef](#)]
35. Kouli, M.; Loupasakis, C.; Soupios, P.; Rozos, D.; Vallianatos, F. Landslide susceptibility mapping by comparing the WLC and WofE multi-criteria methods in the West Crete Island, Greece. *Environ. Earth Sci.* **2014**, *72*, 5197–5219. [[CrossRef](#)]
36. Zhu, C.; Wang, X.; Soc, I.C. Landslide susceptibility mapping: A comparison of information and weights-of-evidence methods in Three Gorges Area. In Proceedings of the International Conference on Environmental Science and Information Application Technology (ESIAT 2009), Wuhan, China, 04–05 July 2009; pp. 342–346.
37. Can, A.; Dagdelenler, G.; Ercanoglu, M.; Sonmez, H. Landslide susceptibility mapping at Ovacik-Karabuk (Turkey) using different artificial neural network models: Comparison of training algorithms. *Bull. Eng. Geol. Environ.* **2019**, *78*, 89–102. [[CrossRef](#)]
38. Huang, Y.; Zhao, L. Review on landslide susceptibility mapping using support vector machines. *Catena* **2018**, *165*, 520–529. [[CrossRef](#)]
39. Niu, C. Index Selection and Rating for Debris Flow Hazard Assessment. Ph.D Thesis, Jilin University, Changchun, China, 2013.
40. Ding, Y. Correlation between landslides and seismides and seismic parameters and its application in predicting slope earthquake disaster. *Chin. J. Geophys.* **1999**. [[CrossRef](#)]
41. Chen, J.; Peng, W.; Sun, X.; Wang, Q.; Han, X. Comparisons of several methods for landslide susceptibility mapping: Case of the Benzilan and Waka Towns, Southwest China. *Arab. J. Geosci.* **2021**, *14*, 1622. [[CrossRef](#)]
42. O'Brien, R.M. A caution regarding rules of thumb for variance inflation factors. *Qual. Quant.* **2007**, *41*, 673–690. [[CrossRef](#)]
43. Quan, H.-C.; Jin, G.-r.; Destech Publicat, I. Landslide Susceptibility Mapping in Changbai Mountain Area Using GIS and Artificial Neural Network (ANN). In Proceedings of the International Conference on GIS and Resource Management (ICGRM), Guangzhou, China, 3–5 January 2014; pp. 174–179.
44. Su, Q.; Zhang, J.; Zhao, S.; Wang, L.; Liu, J.; Guo, J. Comparative Assessment of Three Nonlinear Approaches for Landslide Susceptibility Mapping in a Coal Mine Area. *Isprs Int. J. Geo-Inf.* **2017**, *6*, 228. [[CrossRef](#)]
45. Guru, B.; Veerappan, R.; Sangma, F.; Bera, S. Comparison of probabilistic and expert-based models in landslide susceptibility zonation mapping in part of Nilgiri District, Tamil Nadu, India. *Spat. Inf. Res.* **2017**, *25*, 757–768. [[CrossRef](#)]
46. Zhang, Z.; Yang, F.; Chen, H.; Wu, Y.; Li, T.; Li, W.; Wang, Q.; Liu, P. GIS-based landslide susceptibility analysis using frequency ratio and evidential belief function models. *Environ. Earth Sci.* **2016**, *75*, 948. [[CrossRef](#)]
47. Yu, C. Study on risk mapping of typical geological hazards and comprehensive evaluation of geological environment carrying capacity in Helong City. Ph.D Thesis, Jilin University, Changchun, China, 2021.